



Potential flood-prone area identification and mapping using GIS-based multi-criteria decision-making and analytical hierarchy process in Dega Damot district, northwestern Ethiopia

Ajanaw Negese¹ · Dessalegn Worku¹ · Alazar Shitaye¹ · Haile Getnet¹

Received: 8 August 2022 / Accepted: 29 September 2022 / Published online: 18 October 2022
© The Author(s) 2022

Abstract

Flood is one of the natural hazards that causes widespread destruction such as huge infrastructural damages, considerable economic losses, and social disturbances across the world in general and in Ethiopia, in particular. Dega Damot is one of the most vulnerable districts in Ethiopia to flood hazards, and no previous studies were undertaken to map flood-prone areas in the district despite flood-prone areas identification and mapping being crucial tasks for the residents and decision-makers to reduce and manage the risk of flood. Hence, this study aimed to identify and map flood-prone areas in Dega Damot district, northwestern Ethiopia, using the integration of Geographic Information System and multi-criteria decision-making method with analytical hierarchy process. Flood-controlling factors such as elevation, slope, flow accumulation, distance from rivers, annual rainfall, drainage density, topographic wetness index, land use and land cover, Normalized Difference Vegetation Index, soil type, and curvature were weighted and overlaid together to achieve the objective of the study. The result shows that about 86.83% of the study area has moderate to very high susceptibility to flooding, and 13.17% of the study area has low susceptibility to flooding. The northeastern and southwestern parts of the study area dominated by low elevation and slope, high drainage density, flow accumulation, topographic wetness index, and cropland land use were found to be more susceptible areas to flood hazards. The final flood susceptibility map generated by the model was found to be consistent with the historical flood events on the ground in the study area, revealing the method's effectiveness used in the study to identify and map areas susceptible to flood.

Keywords Flood · Susceptibility to flood hazard · Geographic information system · Multi-criteria decision-making · AHP · Dega damot district

Introduction

Flood is one of the natural disasters that causes massive destruction such as enormous infrastructural damages, substantial economic losses, and social disturbances across the

world (Dang and Kumar 2017; Das and Gupta 2021; Farhadi and Najafzadeh 2021; Hong et al. 2018a, b). The destruction due to floods has increased in recent years in several countries around the world because of climate change and environmental degradation caused by improper land use management (Das and Gupta 2021; Hagos et al. 2022; Kanani-Sadat et al. 2019; Ozkan and Tarhan 2016).

In Ethiopia, flood is one of the major natural hazards which causes significant damage to the lives, livelihoods, and property in different parts of the country (World Bank 2019; NDRMC 2018). According to the United Nations Office for Disaster Risk Reduction (UNDRR 2022), flood and drought are the most recurrent natural disasters in Ethiopia caused by extreme weather events. Flooding in the country is mainly related to prolonged heavy rainfall and the topography of the highlands and lowland plains with

✉ Ajanaw Negese
ajanawnegese@gmail.com
Dessalegn Worku
desuworku60@gmail.com
Alazar Shitaye
alazarshitaye@gmail.com
Haile Getnet
haile2g@gmail.com

¹ Department of Soil Resource and Watershed Management, Woldia University, P.O. Box: 400, Woldia, Ethiopia

natural drainage systems formed by the principal river basins (NDRMC 2018).

The National Disaster Risk Management Commission of Ethiopia (NDRMC 2018, 2020) identified Dega Damot (the study area) and Bahir Dar Zuria districts from West Gojjam Zone of Amhara National Regional State as flood risk areas during rainy seasons. Hence, this study aimed to identify and map areas susceptible to flood in Dega Damot district. No previous studies were undertaken to identify and map flood-prone areas in the district despite the district being recognized as a flood risk area in northwestern Ethiopia.

Sustainable management of flood risk is dependent upon the development of knowledge of the risk and probability of flood events (Binns 2022). In recent years, potential flood risk area mapping is considered as the major strategic component to effectively manage, reduce and mitigate the potential impacts of flood hazards since the maps can provide residents and stakeholders with information on potential flood-prone areas (Abdelkarim et al. 2020; Rahmati et al. 2015).

Different methods and models were developed by previous researchers to investigate and map flood hazards. In recent years, the integrated use of geospatial technologies (GIS and remote sensing) with other models/methods has become the most popular method to examine flood hazards. Multi-criteria decision analysis (MCDA) using analytical hierarchy process (AHP) (Ajibade et al. 2021; Allafta and Opp 2021; Aydin and Birincioğlu 2022; Das and Gupta 2021; Karymbalis et al. 2021; Wubalem et al. 2021), frequency ratio (FR) (Ali et al. 2020; Tehrany et al. 2017; Wubalem et al. 2021; Yariyan et al. 2020), hydrologic engineering centers river analysis system (HEC-RAS) (Demir and Kisi 2016), fuzzy logic (Ajibade et al. 2021; Kanani-Sadat et al. 2019), logistic regression (LR) (Ali et al. 2020; Tehrany et al. 2017; Wubalem et al. 2021), artificial neural networks (ANN) (Tamiru and Dinka, 2021), fuzzy weights-of-evidence (fuzzy-WofE) (Hong et al. 2018a, b; Tehrany et al. 2017), support vector machine (SVM) (Son et al. 2021), random forest (RF) (Farhadi and Najafzadeh, 2021; Son et al. 2021; Wang et al. 2015; Zhao et al. 2018), two-dimensional flood routing model (FLO-2D) (Erena et al. 2018), and adaptive neuro-fuzzy inference system (ANFIS) (Hong et al. 2018a, b; Razavi-Termeh et al. 2018) integrated with geospatial technologies (GIS and remote sensing) are the indispensable methods developed and employed by previous researchers for flood hazard area identification and mapping.

Ali et al. (2020) employed the integration of GIS, multi-criteria decision-making (MCDM) approach, bivariate statistics (frequency ratio and statistical index), and logistic regression to identify flood-prone areas of the Topfa river basin in Slovakia. Demir and Kisi (2016) used GIS and Hydrologic Engineering Centers River Analysis System

(HEC-RAS) to produce a flood hazard map of the Mert river basin in Turkey. Hong et al. (2018a, b) used the integration of the fuzzy weight of evidence (fuzzy-WofE), logistic regression (LR), random forest (RF), and support vector machines (SVM) with GIS to produce a flood susceptibility map of Poyang county in China. Razavi-Termeh et al. (2018) integrated adaptive neuro-fuzzy inference systems (ANFIS) with metaheuristic algorithms and GIS to map flood hazards of the Jahrom basin in the Fars Province of Iran. Tehrany et al. (2017) predicted flood-prone areas of Xing Guo in the Southern Jiangxi Province of China using the combination of GIS with standalone frequency ratio, the weight of evidence, and logistic regression methods. Zhao et al. (2018) employed the random forest model to develop a flood susceptibility map of mountainous areas in China.

Many recent previous studies employed the combination of GIS-based multi-criteria decision analysis (MCDA) and analytical hierarchy process (AHP) to identify and map flood-prone areas. For instance, Abdelkarim et al. (2020) integrated the analytic hierarchy process and GIS-based multi-criteria decision analysis to assess flood risk areas in the Al-Shamal Train Pathway of Al-Qurayyat Region, Kingdom of Saudi Arabia. Aydin and Birincioğlu (2022) integrated nine flood-controlling factors to assess flood-risk areas using a GIS-based analytical hierarchy process in the Bitlis Province of Turkey. Desalegn and Mulu (2021) employed the integration of GIS-based multi-criteria decision analysis with AHP to assess and map flood vulnerability in the Fetam watershed, upper Abay basin of Ethiopia. Similarly, Hagos et al. (2022) employed the combination of GIS-based multi-criteria decision analysis and AHP to combine seven flood-controlling factors to assess and map flood-prone areas in the upper Awash River basin of Ethiopia. Furthermore, other researchers (Ajibade et al. 2021; Allafta and Opp 2021; Astutik et al. 2021; Das and Gupta, 2021; Dash and Sar, 2020; Hadipour et al. 2020; Karymbalis et al. 2021; Mahmoud and Gan, 2018; Ogato et al. 2020; Wubalem et al. 2021; Zzaman et al. 2021) also integrated multi-criteria decision analysis (MCDA) and analytical hierarchy process (AHP) with Geographic Information System to identify and map areas prone to flood.

Multi-criteria decision-making (MCDM) has been recognized as a significant method for evaluating complex decision problems which often involve incomparable data or criteria like the identification and mapping of flood-prone areas using several factors (Abdelkarim et al. 2020; Ali et al. 2020; Allafta and Opp, 2021; Karymbalis et al. 2021); and the analytical hierarchy process (AHP) is the most commonly used method in multi-criteria decision-making (Abdelkarim et al. 2020; Das and Gupta, 2021). Hence, in this study, the integration of the GIS-based multi-criteria decision analysis (GIS-MCDA) approach and analytic hierarchy process (AHP) was employed to identify and map flood-prone areas

in the study area with the identification of eleven factors that affect the occurrence of floods, including elevation, flow accumulation, slope, distance from rivers, rainfall, drainage density, topographic wetness index, land use land cover, Normalized Difference Vegetation Index, soil type and curvature of the land surface.

Materials and methods

Study area

Dega Damot district is located in the West Gojjam Zone of Amhara National Regional State, Ethiopia (Fig. 1). It lies between 10°40'51.414" N and 11°05'18.875" N latitude, and 37°28'54.888" E and 37°46'28.574" E longitude. The district is a part of the Northwestern highlands of Ethiopia with an area coverage of 831.23 square kilometers. The landscape of the district is quite diversified. The topography of the district

is characterized by gently sloping level terrains, steep to very steep hillside slopes, and deeply incised V-shaped valleys with an altitude range from 1725 m above sea level (m.a.s.l) in the northeastern part of the district to 3,594 m.a.s.l in the southeastern parts of the district. The district is dissected by several large and small tributaries of the Abay river basin. Gumara is the largest and longest perennial river in the district that drains throughout the year.

According to the agro-climatic zones classification of the Ministry of Agriculture of Ethiopia, Dega (temperate, sub-humid highlands), Woyina Daga (cool humid highlands), and Wurch (cold highlands) are the three agro-climatic zones found in the district. The majority of the district area (71.89%) is characterized by Dega agro-climatic zone (temperate, sub-humid highlands). The remaining 24.83% and 3.28% of the district area are characterized by the Woyina Daga agro-climatic zone (cool, humid highlands) and Wurch (cold highlands) agro-climatic zone, respectively. Woyina Dega agro-climatic zone is found

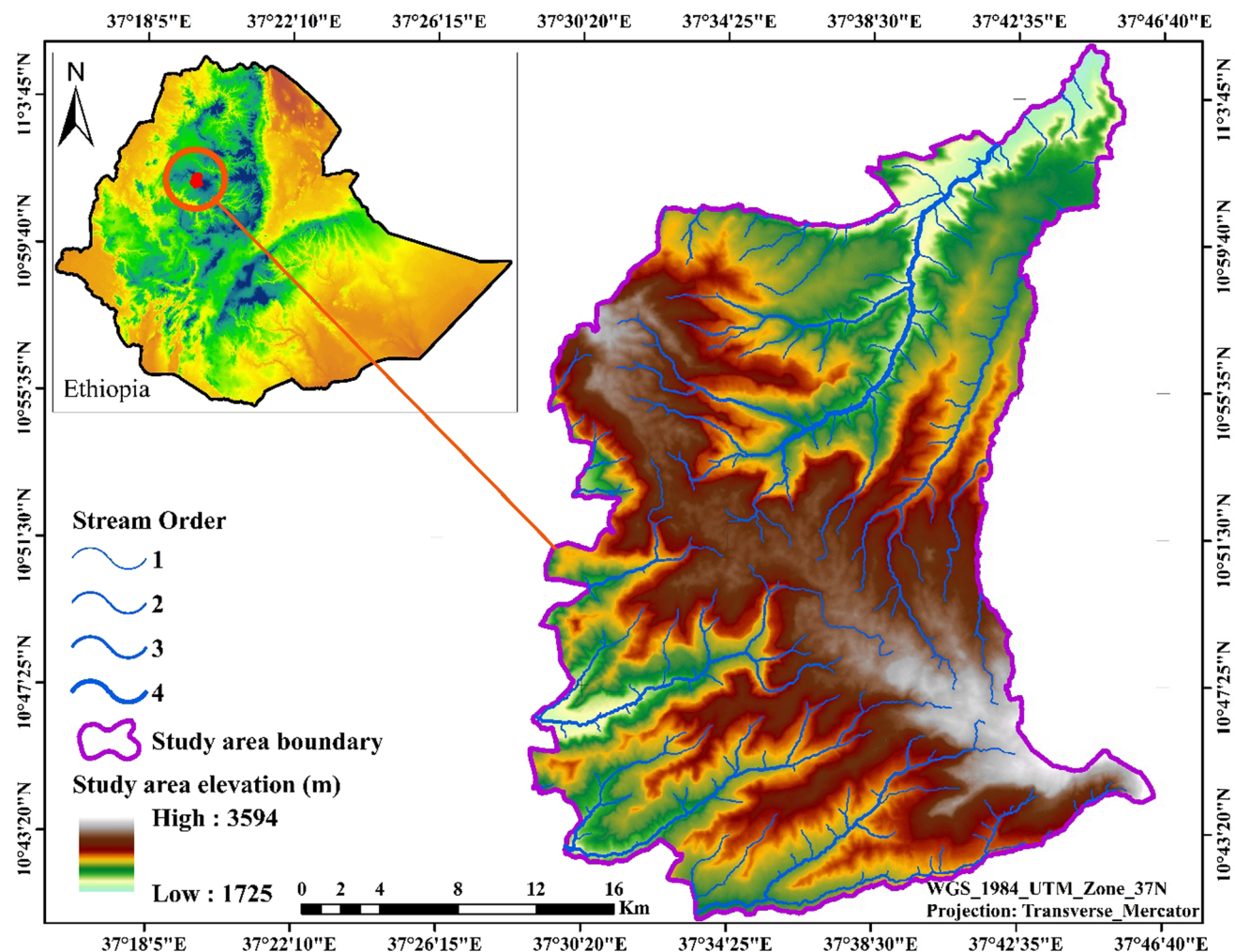


Fig. 1 Location map of the study area

in the southwestern borders and northeastern parts of the district, and the Wurch (cold highlands) agro-climatic zone is found in the southeastern border of the district.

The rainfall data of five meteorology stations (Motta, Feres bet, Digo TSION, Genet Abo, and Dembecha) obtained from the National Meteorological Agency of Ethiopia show that the mean annual rainfall of the district varies from 1306.2 to 1643.2 mm. The district receives its maximum rainfall during the summer season (locally known as kiremt) which extends from June to August. The annual mean minimum and mean maximum temperatures of the district are 10°C and 21°C, respectively, with maximum temperatures in the district occurring from February to May.

The digital soil map (Fig. 5a) obtained from the Ministry of Water, Irrigation, and Energy of Ethiopia shows that Chromic Luvisols, Eutric Cambisols, Lithosols (now Leptosols), Chromic Vertisols, Pellic Vertisols, and Eutric Nitisols are the soil types found in the study area. Chromic Luvisols is the dominant soil type which covers an area of about 38,233.71 ha (46%) of the total area of the district followed by Eutric Cambisols and Eutric Nitisols which covers an area of 21,665.32 ha (26.07%) and 13,776.60 ha (16.57%), respectively.

The data obtained from Environmental System Research Institute (ESRI) show that dense vegetation, shrubland, grassland, cropland, bare land, built area, and water body are the land use and land cover (LULC) types in the district. Cropland shares the greatest size of all other land use types accounting for an area of 67,886.52 ha (81.67%) followed by dense vegetation and shrubland which accounts for about 6,335.34 ha (7.62%) and 5,570 ha (6.70%) of the total area of the district, respectively. Climatically, the district is conducive to the production of different cereal and vegetable crops. Ethiopian teff, maize, barley, potato, bean, pea, and onion are the major crops grown in the district during the rainy season.

Data types and sources

The required data for this study were collected from different sources (Table 1). STRM GDEM Digital Elevation Model with 30 m spatial resolution was downloaded from the U.S Geologic Survey website for the retrieval of different flood-controlling factors. Sentinel 2A satellite image with a spatial resolution of 10 m acquired on 27 March 2022 was also downloaded from the U.S Geologic Survey website. The near-infrared and red bands of the satellite image were used to prepare the Normalized Difference Vegetation Index (NDVI) factor map. The acquisition date of the Sentinel 2A image was purposively selected to reduce the atmospheric effect since the season is dry with the lowest percent or zero monthly cloud cover. A high-quality and accurate Sentinel 2 land use and land cover (LULC) map of 2021 with 10 m spatial resolution was downloaded from the Environmental System Research Institute (ESRI) website. Precipitation data (1995–2020) of five meteorology stations (Feres bet, Motta, Genet Abo, Digo TSION, and Dembecha) were collected from the National Meteorological Agency (NMA) of Ethiopia. The digital soil map of the district was obtained from the Ethiopian Ministry of Water, Irrigation, and Energy. The river map of the district with 15 arc-second resolutions was downloaded from the HydroSHEDS website.

Methods

The integration of GIS-based multi-criteria decision-making (MCDM) and analytical hierarchy process (AHP) was used to identify and map potential areas vulnerable to flood in the study area. Spatial data layers of the eleven factors that affect the occurrence of floods such as elevation (E1), the slope of the land (S1), flow accumulation (FA), distance to rivers (DR), rainfall (Rf), drainage density (DD), topographic wetness index (TWI), land use land cover (LULC), Normalized Difference Vegetation Index (NDVI), soil type (ST) and curvature of the land surface (Cu) were prepared in a raster format by using GIS and remote sensing techniques from the data collected from different sources (Fig. 2).

Table 1 Data types and sources used to map flood-prone areas

Data types	Data Sources
STRM DEM Digital Elevation Model (30 m spatial resolution)	Downloaded from U.S Geologic Survey (http://earthexplorer.usgs.gov/)
Digital Soil Map of the District (1:250,000 scale)	Ethiopian Ministry of Water, Irrigation, and Energy
Sentinel 2 10 m spatial resolution Land Use/Land Cover (LULC) Map (2021)	Environmental System Research Institute (ESRI) (https://livingatlas.arcgis.com/landcover/)
Monthly Rainfall Data (1995–2020)	National Meteorological Agency (NMA) of Ethiopia
Sentinel 2A satellite image (10 m spatial resolution) (acquired on 27 March 2022)	Downloaded from U.S Geologic Survey (http://earthexplorer.usgs.gov/)
River map of the study area with 15 arc-second resolution	Downloaded from the HydroSHEDS website (https://www.hydrosheds.org/)

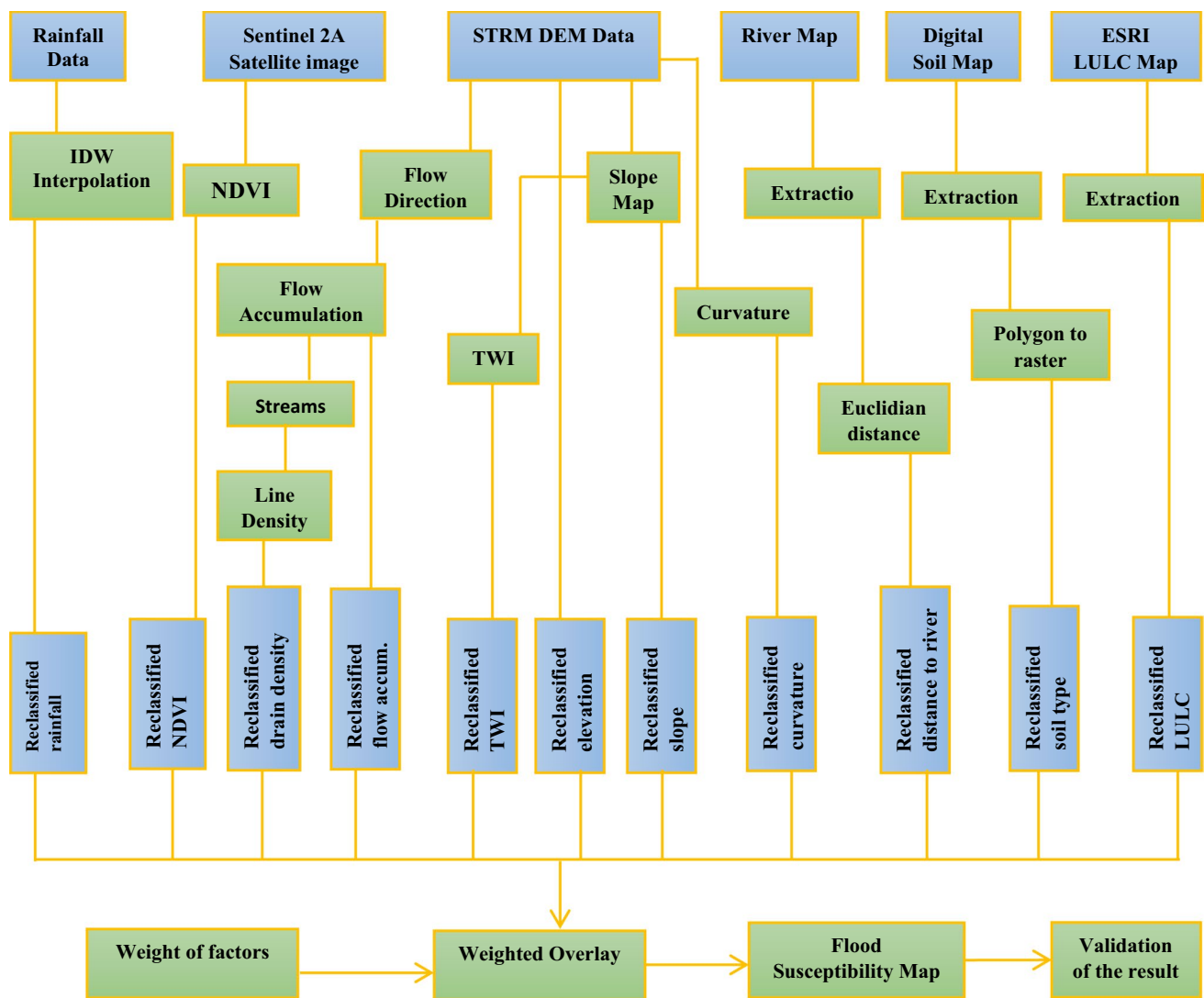


Fig. 2 Flowchart of the methods used to identify and map flood-prone areas

All raster factor maps were reclassified to a common measurement scale from 1 (very low) to 5 (very high) using Reclassify tool of Spatial Analyst Tools and rescaled to 10 m spatial resolution using Resample tool of Data Management Tools in the ArcGIS environment. After the reclassification of all flood-controlling factor maps, analytical hierarchy process (AHP) model was applied to assign a relative weight of influence to each factor. The final flood susceptibility map of the district was derived by overlaying the eleven flood-controlling spatial layers using the weighted overlay method in the ArcGIS environment. ArcGIS 10.8 and ERDAS IMAGINE 2014, and Microsoft Excel software were exhaustively used to process, create, and overlay digital raster layers, and for AHP analysis, respectively.

Methods of flood-controlling factors map preparation and reclassification

The factors to be considered in flood susceptibility mapping using multi-criteria decision-making (MCDM) are not fixed, and there is no common guideline to select the factors. For this study, eleven factors closely associated with flood occurrence were selected based on the assessment of previous studies, data availability, expert opinion, as well as the physical and natural setup of the study area. The factors considered for this study and the methods employed to process/prepare each factor map are described below.

The digital elevation model (DEM) (raster representation of a continuous surface where each cell represents the elevation of a particular location) map of the district has been

reclassified into five flood susceptibility classes and rescaled to a 10-m spatial resolution to create an elevation factor map. The slope and the curvature maps were directly derived from the DEM map of the study area using the slope and curvature tools, respectively, in the Spatial Analyst Tools of the ArcGIS environment.

The DEM map of the district was filled to create free of sinks/depressionless DEM, and then, the flow direction (the direction the stream flows in each cell) map was derived from the filled DEM map. Next, the flow accumulation raster map was created from the flow direction map. Filling the DEM map, creating flow direction, and computing flow accumulation were performed using Hydrology tools such as Fill, Flow Direction, and Flow Accumulation, respectively, in the Spatial Analyst Tools of ArcGIS software.

Since there is only one meteorology station (Feres bet) in the study area, the rainfall record of the other four nearby meteorology stations such as Motta, Genet Abo, Digo Tsion, and Dembecha was used to prepare the rainfall factor map. Rainfall point data of five meteorology stations with their mean annual rainfall were created by importing the data into ArcGIS software from the data obtained from the National Meteorology Agency of Ethiopia. Then, the mean annual rainfall of the five stations was interpolated by Inverse Distance Weighted (IDW) method in the ArcGIS10.8 environment with a cell size of 10 m and clipped using the district boundary shapefile to generate a continuous rainfall map of the district.

The drainage network map was created from the flow accumulation map using the Raster Calculator tool in the ArcGIS environment, and later, the drainage density map was derived from the drainage network map using the Line Density tool in the Spatial Analyst Tools of ArcGIS 10.8 software. The Euclidean Distance tool in the Spatial Analyst Tools of ArcGIS environment was used to create distance to the river raster map after the extraction of study area rivers from the river network data downloaded from the HydroSHEDS website.

The Topographic Wetness Index (TWI) map of the district was derived using equation (Eq. 1) suggested by Moore et al. (1991). The Raster Calculator of Spatial Analyst Tools in the ArcGIS environment was used to generate the TWI map.

$$W = \text{Ln} \left(\frac{A_s}{\tan B} \right) \quad (1)$$

where W represents the topographic wetness index, A_s represents the cumulative upslope area draining through a point (per unit contour length), and B represents the local slope angle in degrees.

To develop the LULC factor map, first, the LULC map of the district was extracted from the land use and land cover

(LULC) map downloaded from the ESRI website. Next, appropriate land use and land cover (LULC) class names were assigned to each land use and land cover using ArcGIS software since the classes are assigned by numbers in the downloaded LULC map.

To develop the soil type factor map, primarily, the soil types of the watershed were identified through extraction using ArcGIS 10.8 software from the Digital Soil Map of Ethiopia obtained from the Ethiopian Ministry of Water, Irrigation and Energy (EMWIE), and the extracted vector soil map was converted into a raster format.

The NDVI map of the district was prepared from a Sentinel 2A satellite image downloaded from the U.S Geologic Survey website. The NDVI map was prepared from the Sentinel 2A satellite image by applying equation (Eq. 2) given below using ERDAS IMAGINE 2014 software.

$$\text{NDVI} = \frac{(\text{NIR} - \text{RED})}{(\text{NIR} + \text{RED})} = \frac{(\text{Band 8} - \text{Band 4})}{(\text{Band 8} + \text{Band 4})} \quad (2)$$

where NDVI is the Normalized Difference Vegetation Index, NIR is surface spectral reflectance in the near-infrared band (which is band 8 in the Sentinel 2A satellite image) and RED is surface spectral reflectance in the red band (which is band 4 in the Sentinel 2A satellite image).

After the preparation of all flood-controlling factors in raster format, all factors were reclassified into five common measurement scales from 1 (very low susceptibility to flooding) to 5 (very high susceptibility to flooding) and rescaled to the same spatial resolution (10 m). The higher classified ranking value (5) corresponds to areas more susceptible to floods, while the lower value (1) corresponds to those areas less susceptible to floods. Since there is no common reclassification scale of flood-controlling factors, the classes of all factors were determined based on the assessment of previous studies and the local context of the study area.

Analytical hierarchy process (AHP)

The analytical hierarchy process (AHP) suggested by Saaty (1987) is the most commonly used and effective method in the multi-criteria decision-making (MCDM) process to assign the relative importance of each criterion or factor considered in the study, and many different previous studies (Abdelkarim et al. 2020; Ajibade et al. 2021; Allafta and Opp 2021; Astutik et al. 2021; Aydin and Birincioğlu 2022; Danumah et al. 2016; Das and Gupta 2021; Elsheikh et al. 2015; Karymbalis et al. 2021; Mahmoud and Gan 2018; Ogato et al. 2020) have employed this method to weight each flood-controlling factors and, finally, to identify and map flood-prone areas.

The factors employed for flood susceptibility mapping using multi-criteria decision-making were given weights

based on the local physical characteristics of the study area and assessment of previous studies. As suggested by Saaty (1987), the following step-by-step procedures were employed to assign relative weights for each flood-controlling factor used in this study.

1. Based on the relative importance, a value ranging from 1 to 9 was assigned to each factor to construct the pairwise comparison matrix (Table 3). According to the scale, 1 refers to equal importance and 9 refers to extreme importance.
2. Next, the normalized pairwise comparison matrix table (Table 4) was prepared by dividing each value in the column in the pairwise comparison matrix by the sum of the column.
3. In the third stage, the weight of each factor was computed (Table 4) by dividing the sum of each row in the normalized pairwise comparison matrix table by the number of factors (which is eleven for this study).

After the computation of weights for each flood-controlling factor, the consistency check was performed using the equations given below to check whether the comparison is correct/consistent or not. The consistency index (CI) is calculated using the following equation (Eq. 3) as given by Saaty (1987).

$$CI = \frac{\lambda_{\max} - n}{n - 1} \quad (3)$$

where CI is the consistency index, n is the number of factors being compared in the matrix, and λ_{\max} is the highest eigenvalue of the pairwise comparison matrix.

As suggested by Saaty (1987), the maximum eigenvalue (λ_{\max}) of the comparison matrix was calculated (Table 5) by the following procedures:

1. multiplying each value in the column (in the matrix table which is not normalized) by the criteria weight
2. computing the weighted sum value by adding the values in the rows
3. calculating the ratio of each weighted sum value to the respective criteria weight, and
4. averaging the ratio of the weighted sum value to the criteria weight

Finally, the consistency ratio (CR) was computed using the following equation (Eq. 4) suggested by Saaty (1987) to verify the consistency of the comparison.

$$CR = \frac{CI}{RI} \quad (4)$$

where CR is the consistency ratio, CI is the consistency index, and RI is the random index which varies according to the number of factors used in the pairwise comparison matrix. If the CR is below 0.10, it means that the pairwise comparison matrix has an acceptable consistency. Otherwise, if the CR is greater than or equal to 0.10, it means that pairwise comparison has inadequate consistency, and the comparison process must be repeated until the value of CR is achieved below 0.10 (Saaty 1987).

Method of flood susceptibility map preparation

After the preparation and reclassification of each flood-controlling factor to a common measurement scale of 1 (very low) to 5 (very high) using ArcGIS software and weighting of the factors using the AHP approach, the spatial layers were integrated and overlaid together in the Spatial Analyst Extension of the ArcGIS environment using the weighted overlay technique by applying equation (Eq. 5) given below to derive the flood susceptibility map of the study area. Many previous studies (Ali et al. 2020; Allafta and Opp 2021; Aydin and Birincioğlu 2022; Das and Gupta 2021; Dash and Sar 2020; Hadipour et al. 2020; Kanani-Sadat et al. 2019) employed this equation (Eq. 5) to generate the flood vulnerability map.

$$FS = \sum_{i=0}^n x_i * w_i \quad (5)$$

where FS is the flood susceptibility, n is the number of decision criteria, x_i is the particular normalized criterion, and w_i is the respective weight of the criterion. The cell/pixel values of the raster layers are multiplied by their weight/percentage influence obtained by AHP analysis, and the results are added together to create the flood susceptibility output raster map.

Results and discussion

Flood-controlling factors processing

The eleven flood-controlling factors used in the study such as elevation, slope, flow accumulation, distance from rivers, rainfall, drainage density, topographic wetness index, land use and land cover, Normalized Difference Vegetation Index, soil type, and curvature of the land surface were used to identify and map potential areas susceptible to flood inundation. By studying and analyzing these factors, the spatial distribution of flood susceptibility in the study area was identified and mapped. More details of the analysis of each factor are presented below.

Elevation

One of the factors used to assess flood risk is elevation. Generally, the lower elevated areas have a higher probability of flood occurrences compared to higher elevated areas because lower elevated areas have comparatively higher river discharge and get flooded faster by the flow of high water (Hong et al. 2018a, b; Lee and Rezaie, 2022; Zzaman et al. 2021). The altitude of the study area ranges from 1725 to 3594 m above sea level. As shown in Fig. 3a, areas with low elevation which are located in the northeastern and southwestern parts of the study area (altitude below 2500 m above sea level) are the most vulnerable areas to flood inundation. On the other hand, areas over central parts which extends from southeastern to northwestern parts of the district (altitude above 2800 m above sea level) have low and very low susceptibility to flooding. About 13.97% (11,612.52 ha) and 32.57% (27,074.88 ha) of the study area have a very high and high susceptibility to flooding inundation, respectively (Table 2).

Slope

The slope of the land controls the velocity of surface water flow. As the slope decreases, the velocity of surface water flow decreases, and the amount of water over the land and the probability of a flood increases (Astutik et al. 2021; Das and Gupta 2021; Zzaman et al. 2021). Mountain areas generally have steeper slopes that prevent the collection of water, whereas lowlands or flatlands with gentle slopes have a higher probability of flood inundation (Wang et al. 2015). The reclassified slope map (Fig. 3b) shows that about 58.16% (48,348 ha) of the study area has a slope range from 0 to 15 degrees which belongs to very high susceptibility to flooding inundation. About 33.67% (27986.22 ha) and 7.83% (6512.04 ha) of the study area are characterized by high (15–30°) and moderate (30–45°) susceptibility to flooding, respectively. Areas of low (45–60°) and very low (60–68.84°) flood susceptibility cover about 0.32% and 0.01%, respectively (Table 2). Gently sloping areas are found in the northeastern, central, and southwestern borders of the study area. Similarly, Yariyan et al. (2020) considered slopes from 0 to 15, 15 to 30, 30 to 45, 45–60, and > 60 degrees as very high, high, moderate, low, and very low susceptibility to floods, respectively.

Flow accumulation

Flow accumulation highlights the amount of flow accumulated in each raster pixel based on the cumulative weights of the preceding pixels (Ajibade et al. 2021). Flow accumulation is probably the most important parameter for delineating flood-prone areas (Kazakis et al. 2015). It helps us

to map out the convergence zone of surface runoff. High flow accumulation means that the area is more likely to be flooded (Kazakis et al. 2015; Mahmoud and Gan, 2018). In this study, the reclassification used by Mahmoud and Gan (2018) was adopted to reclassify the flow accumulation of the study area into five classes. Hence, as shown in Fig. 3c and Table 2, the flow accumulation values are classified into five categories: very low (< 250 pixels), low (250–2195 pixels), moderate (2195–3415 pixels), high (3415–15,125 pixels) and very high (> 15,125 pixels). The red and blue pixels (Fig. 3c) represent areas with very high and high flow accumulation, respectively, while the yellow and light blue pixels represent areas with low and very low flow accumulation, respectively. The higher the flow accumulation values in the area, the more vulnerable it is to flooding.

Rainfall

The consideration of rainfall as a factor in flood susceptibility analysis is a must since we cannot think about flood occurrence without it. It is the most crucial triggering factor for the occurrence of floods because flood inundation is due to a huge volume of runoff flows as a result of excessive heavy rainfall or prolonged rainfall (Allafta and Opp 2021; Hong et al. 2018a, b). The mean annual rainfall of the district varies from 1306.18 to 1643.19 mm/year and reclassified (1306.18–1338 mm), (1338–1433 mm), (1433–1513 mm), (1513–1618 mm), and (1618–1643.19 mm) as very low, low, moderate, high, and very high contribution to flooding, respectively. The classification adopted by Das and Gupta (2021) was used to reclassify the rainfall map of the study area. As shown in Fig. 3d, the western parts of the study area are the most susceptible parts to flood inundation compared to the eastern parts. About 1.94%, 27.13%, 35.04%, 35.57%, and 0.33% of the study areas were classified as very low, low, moderate, high, and very high vulnerability to flooding, respectively (Table 2).

Distance from the river

Areas that are close to rivers have a higher probability of flood inundation than areas located far away from the rivers since surplus water from the rivers initially reaches alongside river banks and adjoining lowland areas (Mahmoud and Gan 2018). This is because as the distance increases, the slope and elevation become higher (Lee and Rezaie 2022; Zzaman et al. 2021). In the study area, areas that are within a distance of 500 m from the river are categorized as very highly susceptible to flooding, while areas within a distance of 1000, 1500, 2000, and > 2000 m from the river are considered to have high, moderate, low, and very low vulnerability to flooding, respectively (Fig. 4a and Table 2). Similarly, a study conducted by Shadmehri Toosi et al. (2019) and

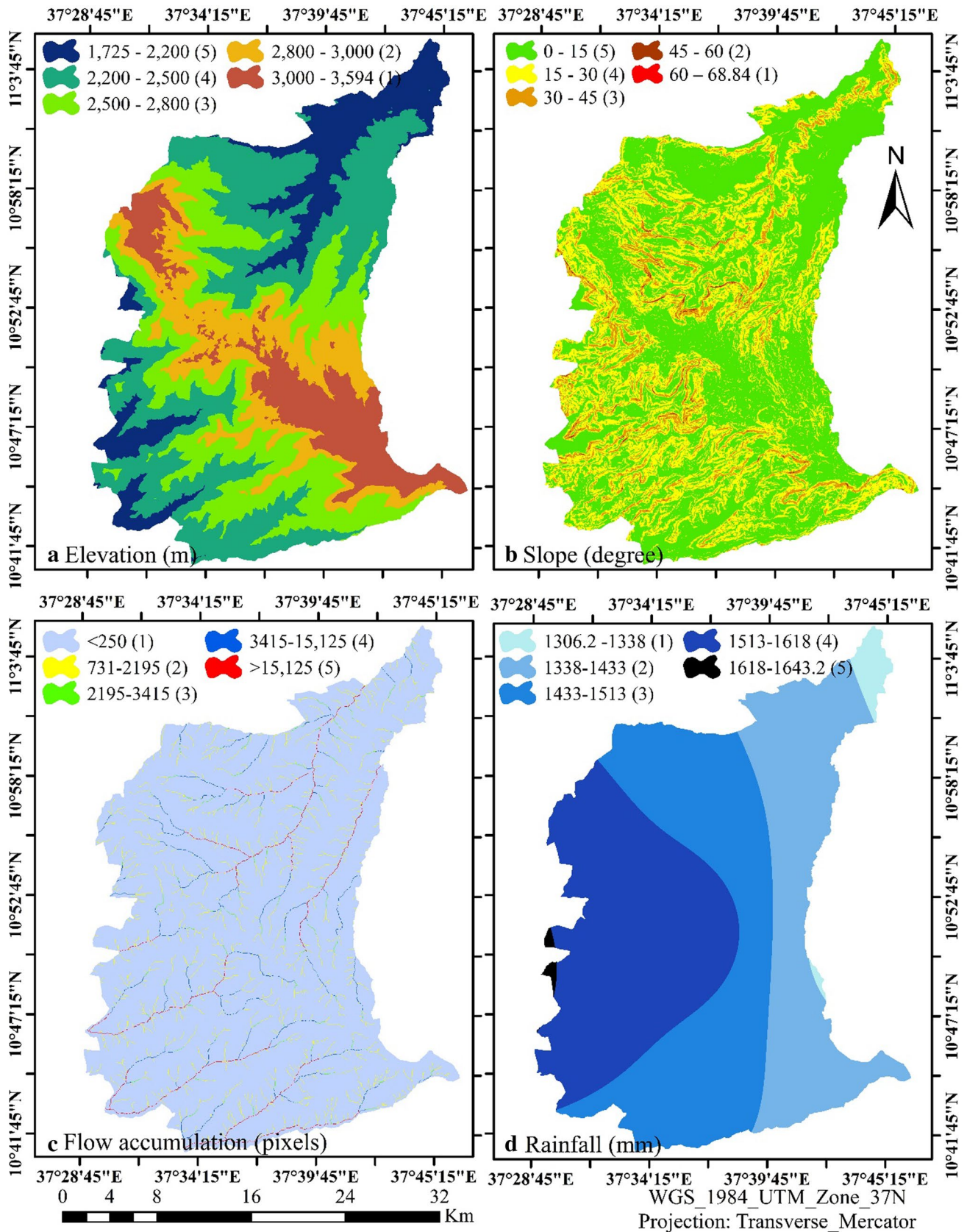


Fig. 3 Elevation a, slope b, flow accumulation c and rainfall d factor maps

Table 2 Flood conditioning factors, their classes, rating values, area coverage, and percentage

Factor	Class	Flood susceptibility	Rating	Class pixels	Area	
					ha	Percent (%)
Elevation (El) (m)	1725–2200	Very high	5	1,161,252	11,612.52	13.97
	2200–2500	High	4	2,707,488	27,074.88	32.57
	2500–2800	Moderate	3	2,045,988	20,459.88	24.61
	2800–3000	Low	2	1,345,959	13,459.59	16.19
	3000–3594	Very Low	1	1,051,605	10,516.05	12.65
Slope (Sl) (degree)	0–15	Very high	5	4,834,800	48,348	58.16
	15–30	High	4	2,798,622	27,986.22	33.67
	30–45	Moderate	3	651,204	6,512.04	7.83
	45–60	Low	2	26,469	264.69	0.32
	60–68.84	Very Low	1	1197	11.97	0.01
Flow Accumulation (FA) (pixels)	< 250	Very low	1	8,037,585	8,0375.85	96.70
	250–2195	Low	2	176,652	1,766.52	2.13
	2195–3415	Moderate	3	17,451	174.51	0.21
	3415–15,125	High	4	43,497	434.97	0.52
	> 15,125	Very high	5	37,107	371.07	0.45
Rainfall (Rf) (mm)	1306.18–1338	Very low	1	161,518	1,615.18	1.94
	1338–1433	Low	2	2,255,033	22,550.33	27.13
	1433–1513	Moderate	3	2,912,303	29,123.03	35.04
	1513–1618	High	4	2,956,341	29,563.41	35.57
	1618–1643.19	Very high	5	27,097	270.97	0.33
Distance to the rivers (DR) (m)	0–500	Very high	5	1,595,489	15,954.89	19.19
	500–1000	High	4	1,676,426	16,764.26	20.17
	1000–1500	Moderate	3	1,475,296	14,752.96	17.75
	1500–2000	Low	2	1,317,168	13,171.68	15.85
	2000–6832.92	Very Low	1	2,247,913	22,479.13	27.04
Drainage density (DD) (km/km ²)	0–0.4	Very low	1	2,789,073	27,890.73	33.55
	0.4–1	Low	2	4,089,884	40,898.84	49.20
	1–1.5	Moderate	3	1,328,810	13,288.1	15.99
	1.5–2	High	4	101,758	1,017.58	1.22
	2–2.1	Very high	5	2767	27.67	0.03
Topographic Wetness Index (TWI)	2.48–5.91	Very low	1	3,773,259	37,732.59	45.39
	5.91–8.09	Low	2	3,276,252	32,762.52	39.41
	8.09–10.18	Moderate	3	803,727	8,037.27	9.67
	10.18–12.63	High	4	319,608	3,196.08	3.85
	12.63–22.77	Very high	5	139,446	1,394.46	1.68
Land use/Land cover (LULC)	Dense vegetation	Very low	1	632,736	6,327.36	7.61
	Shrub land	Low	2	557,869	5,578.69	6.71
	Grassland	Moderate	3	119,483	1,194.83	1.44
	Cropland/Bare land	High	4	6,792,448	67,924.48	81.72
	Built Area/Water body	Very high	5	209,756	2,097.56	2.52
Soil Type (ST)	Eutric Cambisols	Very low	1	2,166,242	21,662.42	26.06
	Eutric Nitisols	Low	2	1,376,194	13,761.94	16.56
	Chromic Luvisols	Moderate	3	3,822,611	38,226.11	45.99
	Leptosols	High	4	891,982	8,919.82	10.73
	Chromic/Pellic Vertisols	Very high	5	55,263	552.63	0.66

Table 2 (continued)

Factor	Class	Flood susceptibility	Rating	Class pixels	Area	
					ha	Percent (%)
Normalized Difference Vegetation Index (NDVI)	− 0.16–0.29	Very high	5	7,512,607	75,126.07	90.38
	0.29–0.38	High	4	650,874	6,508.74	7.83
	0.38–0.45	Moderate	3	134,280	1,342.8	1.62
	0.45–0.51	Low	2	13,346	133.46	0.16
	0.51–0.59	Very Low	1	1185	11.85	0.01
Curvature (Cu)	Convex (positive)	Moderate	3	1,804,005	18,040.05	21.70
	Concave (negative)	High	4	1,807,470	18,074.7	21.74
	Flat (close to zero)	Very high	5	4,700,817	47,008.17	56.55

Das and Gupta (2021) considered areas within the distance of 500, 1000, 1500, 2000, and > 2000 m from the river as very high, high, moderate, low, and very low vulnerability to flooding, respectively.

Drainage density

The drainage density represents the ratio of the total length of streams within an area to the size of the area (Zzaman et al. 2021). The higher the drainage density, the higher the surface runoff and the higher the probability of flooding (Abdelkarim et al. 2020; Das and Gupta 2021; Lee and Rezaie 2022; Mahmoud and Gan 2018). A study conducted by Ali et al. (2020) considered areas with drainage density values less than 0.45 km/km², (0.45–1.01 km/km²), (1.01–1.64 km/km²), (1.64–2.47 km/km²) and greater than 2.47 km/km² as very low, low, moderate, high and very high susceptibility to flooding, respectively. Likewise, as shown in Fig. 4b and Table 2, the drainage density value in this study is classified into five categories: very low (0–0.4 km/km²), low (0.4–1 km/km²), moderate (1–1.5 km/km²), high (1.5–2 km/km²) and very high (> 2.1 km/km²). The heavy blue color (Fig. 4b) represents areas with very high drainage density, while the light blue color represents areas with low drainage density.

Topographic wetness index (TWI)

Topographic Wetness Index is an index used to quantify the topographical effect on runoff generation and flow accumulation volume at any given place. It depicts the tendency of water to collect at a given spot or travel downhill due to gravitational pressure (Lee and Rezaie 2022). Topographic Wetness Index is capable to predict areas susceptible to saturated land surfaces and areas that carry the potential to produce overland flow (Hong et al. 2018a, b). The TWI is directly proportional to flood risk; the higher the TWI value, the greater the likelihood of flood inundation (Das and

Gupta 2021). A study conducted by Ali et al. (2020) considered areas with a TWI from 5.57 to 7.58, 7.58 to 8.68, 8.68 to 10.17, 10.17 to 12.63, and 12.63 to 22.09 as very low, low, moderate, high and very high susceptibility to flooding, respectively. Likewise, as shown in Fig. 4c and Table 2, the TWI of the study area was classified into five classes of susceptibility to flooding such as very low (2.48–5.91), low (5.91–8.09), moderate (8.09–10.18), high (10.18–12.63), and very high (12.63–22.77) which covers 45.39%, 39.41%, 9.67%, 3.85% and 1.68% of the study area, respectively.

Land use and land cover (LULC)

One of the most important factors for flood occurrence is land use and land cover. Because vegetation slows the rapid flow of water and induces high infiltration, areas with a high density of vegetation are often less vulnerable to flood risk. In urban and residential areas, on the other hand, runoff increases due to impermeable surfaces and little infiltration (Allafta and Opp 2021; Das and Gupta 2021; Kazakis et al. 2015; Zzaman et al. 2021). Allafta and Opp (2021) considered shrub land, cropland, bare land, urban, and waterbody as very low, low, moderate, high, and very high susceptibility to flooding, respectively. Das and Gupta (2021) categorized waterbody, build-up, agriculture, sparse vegetation, and dense vegetation as very high, high, moderate, low, and very low vulnerability to flooding, respectively. Hagos et al. (2022) also classified built-up areas, farmland, grassland, shrubland, and forestland areas as extremely high, high, moderate, low, and extremely low vulnerability to flooding, respectively. Likewise, the LULC map of the study area (Fig. 4d) in this study is categorized as very high (built area and water body), high (cropland/bare land), moderate (grassland), low (shrubland), and very low (dense vegetation) susceptibility to floods. Crop land is the major LULC type of the district covering about 81.72% of the study area (Fig. 4d and Table 2), representing high susceptibility to

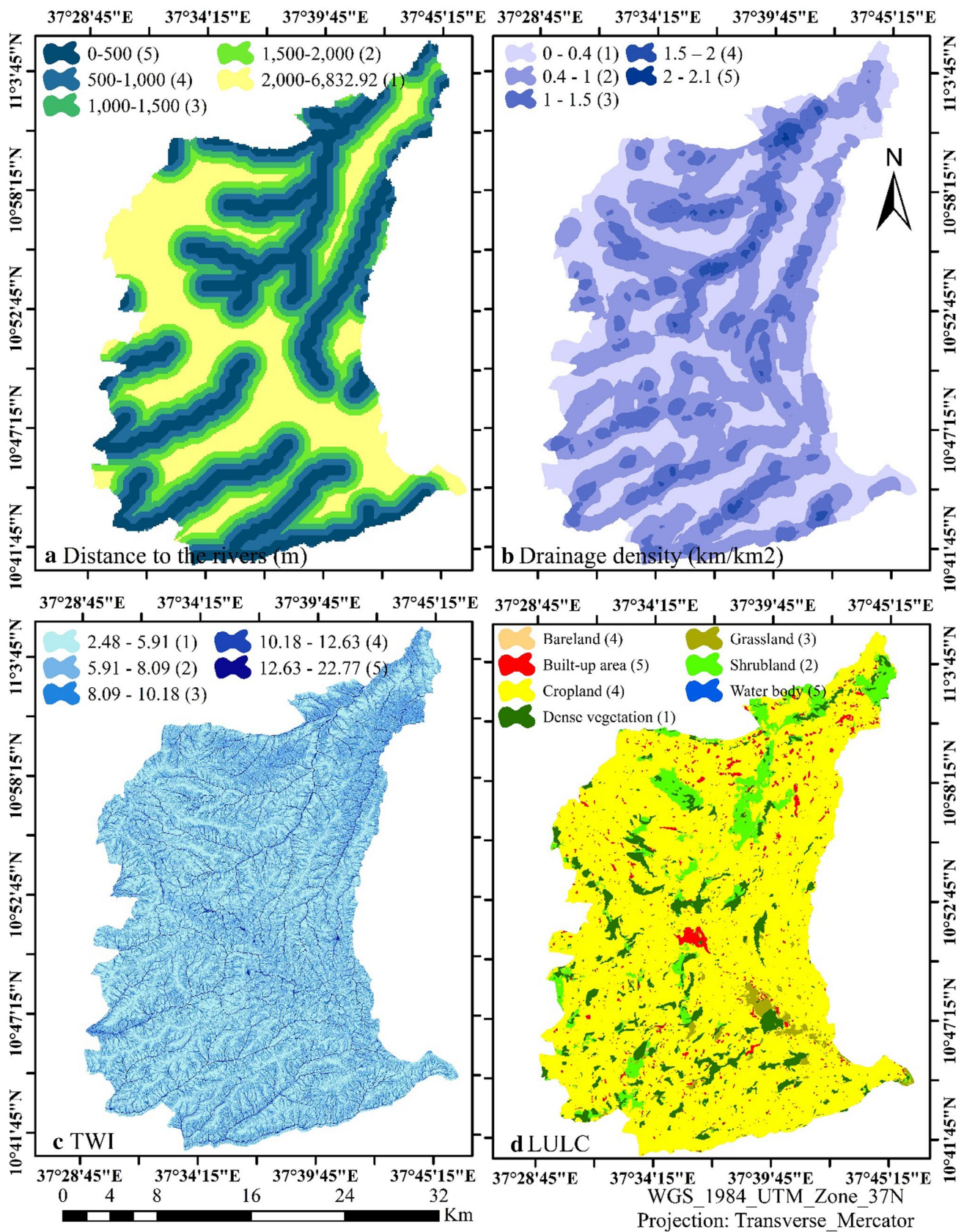


Fig. 4 Distance from the rivers a, drainage density b, Topographic Wetness Index c, and land use/land cover d factor maps

flooding. Dense vegetation and shrubland cover about 7.61% and 6.71%, respectively.

Soil types

The infiltration process is highly dependent on the nature of the soil. The fine texture composition of the soil reduces infiltration and increases surface runoff. Hence, areas covered by fine soil texture are more likely to be flooded than areas with coarse soil texture (Allafta and Opp 2021; Hagos et al. 2022; Hong et al. 2018a, b). As shown in Fig. 5a, the soil types of the study area are classified as very low (Eutric Cambisols), low (Eutric Nitisols), moderate (Chromic Luvisols), high (Leptosols), and very high (Chromic Vertisols and Pellic Vertisols) susceptibility to floods. About 57.38% of the study area is characterized by moderate to very high susceptibility to floods. The rest 16.56% and 26.06% of the study area are characterized by low and very low susceptibility to flooding, respectively (Table 2). Similarly, Ogato et al. (2020) considered areas with Eutric Cambisols, Eutric Nitisols, Chromic Luvisols, Leptosols, and Chromic Vertisols as very low, low, moderate, high, and very high susceptibility to floods, respectively.

Normalized difference vegetation index (NDVI)

Normalized Difference Vegetation Index is an index representing the vegetation density over an area, and it is one of the factors used for determining flood susceptibility (Ali et al. 2020). Higher vegetation density decreases the speed of the runoff and flood inundation (Tehrany et al. 2017). As shown in Fig. 5b, this study considered areas with NDVI values from -0.16 to 0.29 , 0.29 to 0.38 , 0.38 to 0.45 , 0.45 to 0.51 , and 0.51 to 0.59 as very high, high, moderate, low and very low susceptible to flooding, respectively. Areas with high to very high NDVI values are found in the central and southeastern parts of the district. Similarly, a study conducted by Ali et al. (2020) considered areas with NDVI values <0.29 , 0.29 to 0.38 , 0.38 to 0.45 , 0.45 to 0.51 , and >0.51 as very high, high, moderate, low, and very low susceptibility to flooding, respectively. In this study, an NDVI value of less than 0.29 (high susceptibility to flooding) covers about 90.38% of the study area, and 7.83% and 1.62% of the study area have NDVI value 0.29 – 0.38 and 0.38 – 0.45 , respectively.

Curvature

Curvature defines the morphology of the surface topography of an area (Das and Gupta 2021) or it is the rate of slope change in a particular direction (Zzaman et al. 2021). A positive curvature value indicates a convex surface, a negative curvature value indicates a concave surface, and

a value close to zero indicates a flat surface, and the flat curvature is very prone to flooding followed by concave and convex (Astutik et al. 2021; Das and Gupta 2021; Zzaman et al. 2021). As shown in Fig. 5c, the curvature of the earth's surface in this study was classified into three classes: Concave (-19.33 to -0.47), flat (-0.47 to 0.49), and convex (0.49 – 26.22). As shown in Table 2, about 56.55% (47,008.17 ha) and 21.74% (18,074.7 ha) of the research area are characterized by flat and concave curvature, respectively. The remaining 21.70% (18,040.05 ha) of the study area is characterized by convex curvature.

Analytical hierarchy process (AHP) analysis

After the reclassification of each flood-controlling factor (Fig. 6), AHP analysis was performed to assign relative weight or influence of flood-controlling factors subject to weighted overlay. A pairwise comparison matrix was developed (Table 3), the normalization of the pairwise comparison and the weight of the factors was computed (Table 4), and the consistency check of the comparison was performed (Table 5) according to the procedures suggested by Saaty (1987). Table 4 shows the final criteria weight for each flood-controlling factor, which reflects the estimated relative influence of each factor on flooding occurrence in the study area: elevation (17.61%), the slope of the land (15.16%), flow accumulation (14.86%), annual rainfall (11.36%), distance from rivers (11.04%), drainage density (8.13%), topographic wetness index (5.69%), land use and land cover (7.21%), soil type (3.97%), Normalized Difference Vegetation Index (2.82%), and curvature (2.15%). The Consistency Index (CI=0.07) was calculated using Eq. (3), and the consistency ratio (CR=0.05) was computed using Eq. (4). To calculate the CI, the calculated highest eigenvalue ($\lambda_{\max} = 11.72$) and the number of factors ($n = 11$) were used. To calculate CR, the random index (RI) of 1.51 was used. The random index (RI) varies depending on the number of factors and it is 1.51 for eleven factors according to different authors (Abu Dabous and Alkass, 2008; Aydin and Birincioğlu, 2022; Danumah et al. 2016; Weng et al. 2018). The calculated value of consistency ratio (CR) is 0.05 (5%) which is acceptable to use the comparison for weighted overlay since it is less than 0.1 (10%).

Flood susceptibility map of the study area

As shown in Fig. 7, the final flood susceptibility map of Dega Damot district was developed by the integration of eleven flood-controlling factors thematic maps. The weighted overlay integration classified the district into five flood susceptibility classes: very high (5), high (4), moderate (3), low (2), and very low (1) susceptibility. Table 6 shows the estimated area of each susceptibility class: 0.0005%

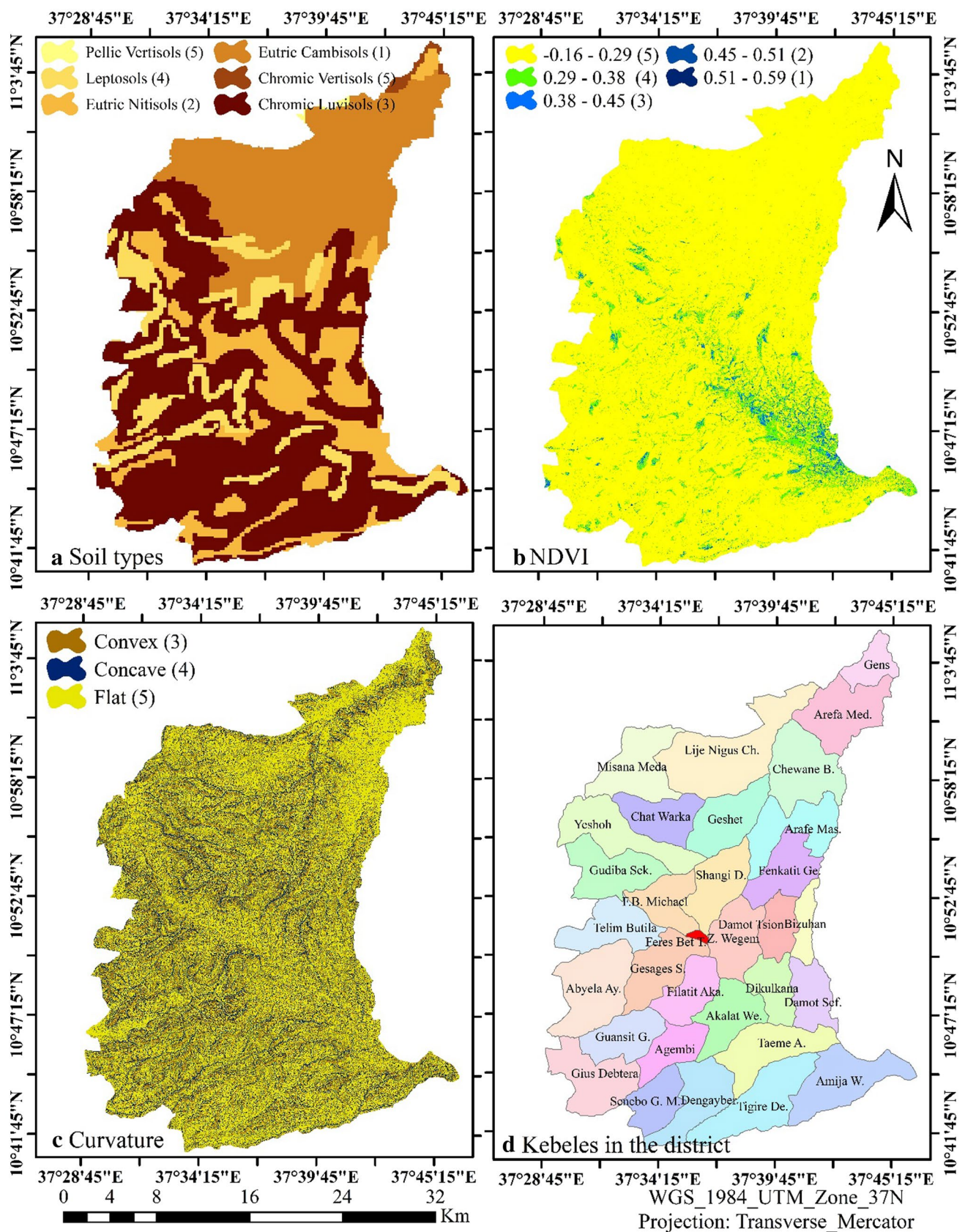


Fig. 5 Soil type a, Normalized Difference Vegetation Index b, surface curvature c, and kebeles of the district d (kebele is the lowest administrative unit in Ethiopia)

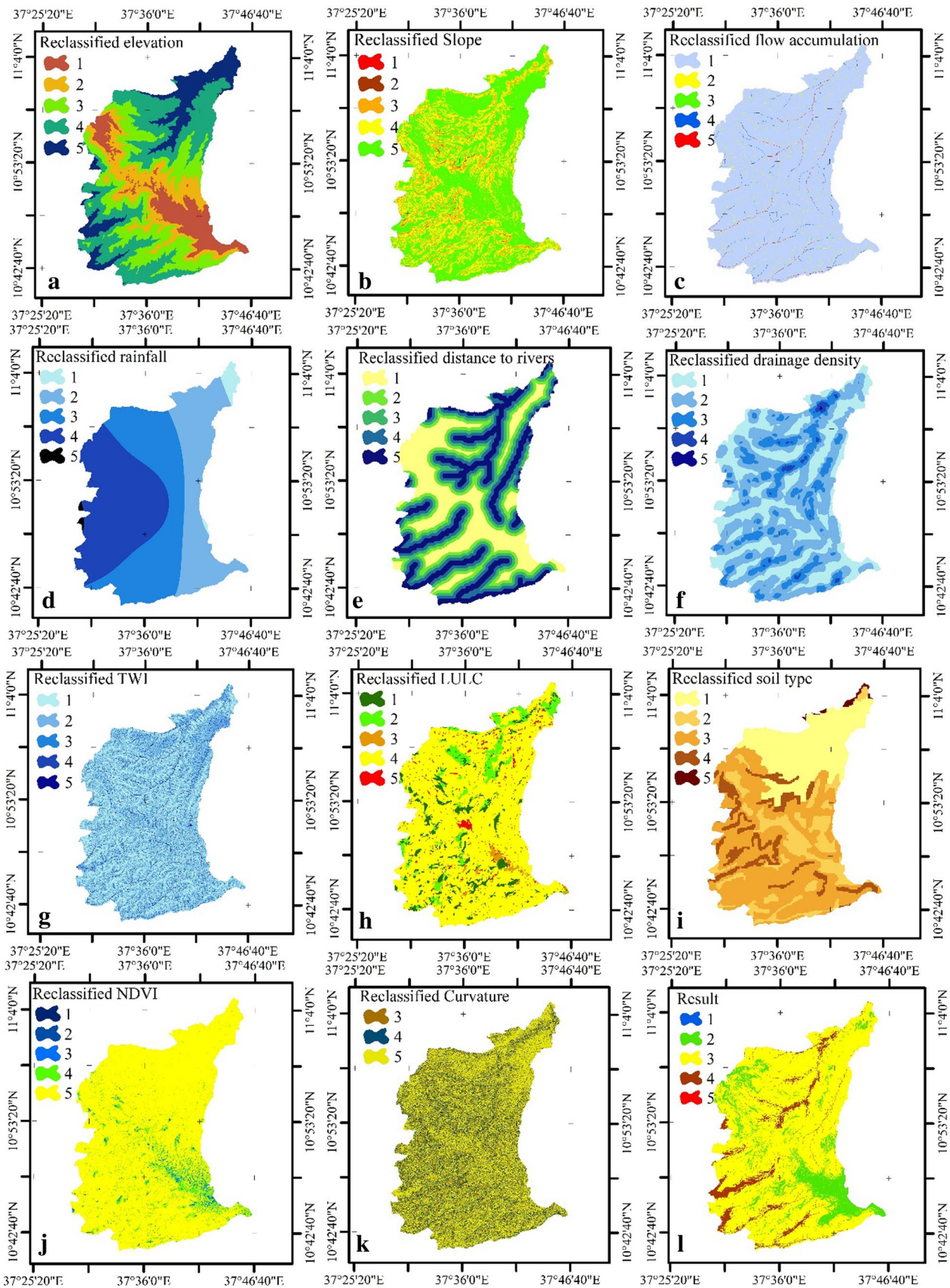


Fig. 6 Reclassification of flood-controlling factors (a-k) and result (l) map

Table 3 Pairwise comparison matrix for selected flood-controlling factors

Factors	El	Sl	FA	Rf	DR	DD	TWI	LULC	ST	NDVI	Cu
El	1	2	2	2	2	3	3	2	3	4	4
Sl	1/2	1	1	3	2	3	3	1	4	5	5
FA	1/2	1	1	2	2	3	3	2	4	4	6
Rf	1/2	1/3	1/2	1	2	2	3	2	3	4	5
DR	1/2	1/2	1/2	1/2	1	2	3	3	4	4	4
DD	1/3	1/3	1/3	1/2	1/2	1	2	2	3	4	5
TWI	1/3	1/3	1/3	1/3	1/3	1/2	1	1	2	3	4
LULC	1/2	1	1/2	1/2	1/3	1/2	1	1	2	3	4
ST	1/3	1/4	1/4	1/3	1/4	1/3	1/2	1/2	1	2	3
NDVI	1/4	1/5	1/4	1/4	1/4	1/4	1/3	1/3	1/2	1	2
Cu	1/4	1/5	1/6	1/5	1/4	1/5	1/4	1/4	1/3	1/2	1

El elevation, *Sl* slope, *FA* flow accumulation, *Rf* annual rainfall, *DR* distance to rivers, *DD* drainage density, *TWI* topographic wetness index, *LULC* land use and land cover, *ST* soil type, *NDVI* Normalized difference vegetation index, and *Cu* curvature

Table 4 Normalized pairwise comparison matrix and calculated criteria weight for each factor

Factors	El	Sl	FA	Rf	DR	DD	TWI	LULC	ST	NDVI	Cu	Sum	CW	CW (%)
El	0.2000	0.2797	0.2927	0.1884	0.1832	0.1901	0.1494	0.1326	0.1118	0.1159	0.0930	1.9368	0.1761	17.61
Sl	0.1000	0.1399	0.1463	0.2826	0.1832	0.1901	0.1494	0.0663	0.1491	0.1449	0.1163	1.6680	0.1516	15.16
FA	0.1000	0.1399	0.1463	0.1884	0.1832	0.1901	0.1494	0.1326	0.1491	0.1159	0.1395	1.6344	0.1486	14.86
Rf	0.1000	0.0466	0.0732	0.0942	0.1832	0.1267	0.1494	0.1326	0.1118	0.1159	0.1163	1.2499	0.1136	11.36
DR	0.1000	0.0699	0.0732	0.0471	0.0916	0.1267	0.1494	0.1989	0.1491	0.1159	0.0930	1.2148	0.1104	11.04
DD	0.0667	0.0466	0.0488	0.0471	0.0458	0.0634	0.0996	0.1326	0.1118	0.1159	0.1163	0.8945	0.0813	8.13
TWI	0.0667	0.0466	0.0488	0.0314	0.0305	0.0317	0.0498	0.0663	0.0745	0.0870	0.0930	0.6263	0.0569	5.69
LULC	0.1000	0.1399	0.0732	0.0471	0.0305	0.0317	0.0498	0.0663	0.0745	0.0870	0.0930	0.7929	0.0721	7.21
ST	0.0667	0.0350	0.0366	0.0314	0.0229	0.0211	0.0249	0.0331	0.0373	0.0580	0.0698	0.4367	0.0397	3.97
NDVI	0.0500	0.0280	0.0366	0.0235	0.0229	0.0158	0.0166	0.0221	0.0186	0.0290	0.0465	0.3097	0.0282	2.82
Cu	0.0500	0.0280	0.0244	0.0188	0.0229	0.0127	0.0124	0.0166	0.0124	0.0145	0.0233	0.2360	0.0215	2.15

CW criteria weight

Table 5 Calculating the consistency of pairwise comparison (CR=0.05)

Factors	El	Sl	FA	Rf	DR	DD	TWI	LULC	ST	NDVI	Cu	WSV	CW	WSV/CW
El	0.1761	0.3033	0.2972	0.2273	0.2209	0.2440	0.1708	0.1442	0.1191	0.1126	0.0858	2.1011	0.1761	11.93
Sl	0.0880	0.1516	0.1486	0.3409	0.2209	0.2440	0.1708	0.0721	0.1588	0.1408	0.1073	1.8437	0.1516	12.16
FA	0.0880	0.1516	0.1486	0.2273	0.2209	0.2440	0.1708	0.1442	0.1588	0.1126	0.1287	1.7954	0.1486	12.08
Rf	0.0880	0.0505	0.0743	0.1136	0.2209	0.1626	0.1708	0.1442	0.1191	0.1126	0.1073	1.3640	0.1136	12.00
DR	0.0880	0.0758	0.0743	0.0568	0.1104	0.1626	0.1708	0.2163	0.1588	0.1126	0.0858	1.3123	0.1104	11.88
Dd	0.0587	0.0505	0.0495	0.0568	0.0552	0.0813	0.1139	0.1442	0.1191	0.1126	0.1073	0.9491	0.0813	11.67
TWI	0.0587	0.0505	0.0495	0.0379	0.0368	0.0407	0.0569	0.0721	0.0794	0.0845	0.0858	0.6528	0.0569	11.47
LULC	0.0880	0.1516	0.0743	0.0568	0.0368	0.0407	0.0569	0.0721	0.0794	0.0845	0.0858	0.8269	0.0721	11.47
ST	0.0587	0.0379	0.0371	0.0379	0.0276	0.0271	0.0285	0.0360	0.0397	0.0563	0.0644	0.4512	0.0397	11.37
NDVI	0.0440	0.0303	0.0371	0.0284	0.0276	0.0203	0.0190	0.0240	0.0198	0.0282	0.0429	0.3217	0.0282	11.43
Cu	0.0440	0.0303	0.0248	0.0227	0.0276	0.0163	0.0142	0.0180	0.0132	0.0141	0.0215	0.2467	0.0215	11.50

WSV weighted sum value, CW criteria weight

Fig. 7 Flood susceptibility map of the study area

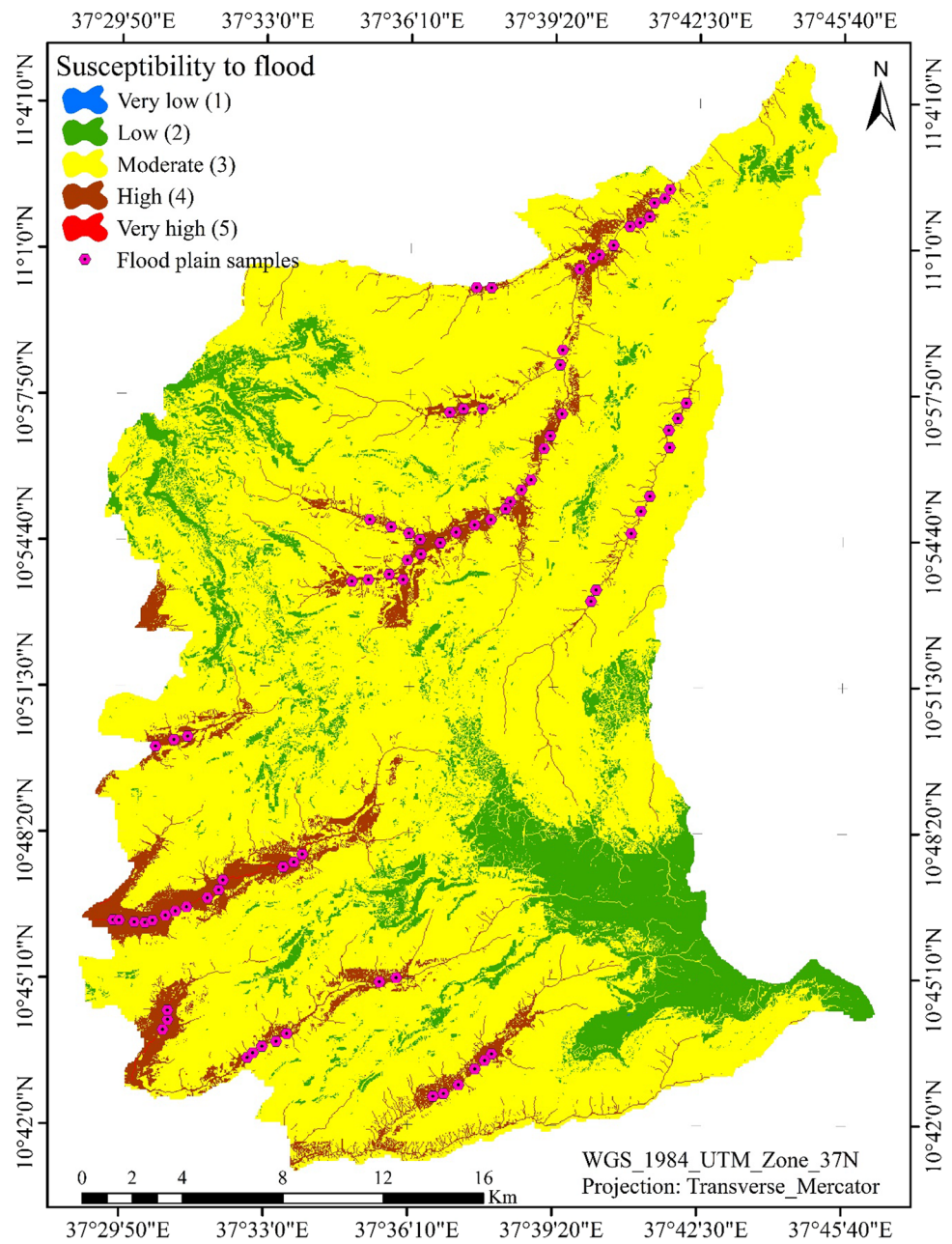


Table 6 Flood susceptibility, area coverage, and percentage

Flood susceptibility	Class pixels	Area	
		ha	Percent (%)
Very low (1)	41	0.41	0.0005
Low (2)	1,095,037	10,950.37	13.17
Moderate (3)	6,515,888	65,158.88	78.39
High (4)	697,325	6,973.25	8.39
Very high (5)	4001	40.01	0.05
Total	8,312,292	83,122.92	100.00

(0.41 ha), 13.17% (10,950.37 ha), 78.39% (65,158.88 ha), 8.39% (6,973.25 ha) and 0.05% (40.01 ha) of the study area are classified as very low, low, moderate, high, and very high susceptibility to flooding, respectively. About 86.83% of the study area is characterized by moderate to very high susceptibility to flooding. The remaining 13.17% of the study area is characterized by low to very low susceptibility to flooding. The flood susceptibility map (Fig. 7) shows that most of the northern, northeastern, southern, and southwestern parts of the study area are the more vulnerable areas to flooding.

The result shows that Arefa Medihanialem, Chewane Bihande, Lije Nigus Chat Warka, Geshet, Arefa Masikena, Fenkatit Gendawuha kebeles, eastern parts of Chat Warka

Table 7 Percentage of flood susceptibility in the kebeles of the district

Kebeles in the District	Area (ha)	Flood Susceptibility area (%) in the kebele				
		Very low (1)	Low (2)	Moderate (3)	High (4)	Very high (5)
Feres Bet Town	1,24.35	–	0.47	99.53	–	–
Arefa Medihanialem	3,309.16	–	2.34	94.90	2.755	–
Genis	1,278.87	–	15.62	82.62	1.763	–
Chewane Bihande	3,514.55	–	3.19	89.45	7.357	–
Lije Nigus Chat Warka	5,732.73	–	2.04	90.15	7.818	–
Meles Misana Meda	3,185.44	–	22.60	76.60	0.806	–
Chat Warka	2,291.04	–	10.96	85.05	3.984	–
Geshet	2,771.80	–	3.31	86.52	10.167	0.01
Arefa Masikena	2,931.32	–	2.27	89.72	8.003	–
Fenkatit Gendawuha	2,418.24	–	2.92	94.21	2.867	–
Shangi Dereke	2,592.26	–	5.77	81.59	12.571	0.06
Santima Yeshoh	3,380.93	–	17.60	79.55	2.853	–
Feres Bet Michael	1,940.75	–	7.36	85.86	6.781	–
Gudiba Sekela	2,930.16	–	16.90	76.26	6.834	–
Telim Butila	2,669.69	–	10.33	83.07	6.52	0.08
Gesagis Shimbirma	2,708.37	–	6.84	79.60	13.28	0.28
Zikuala Wegem	2,482.32	–	14.27	85.09	0.64	–
Damot Tseyion	1,513.19	–	11.75	86.01	2.24	–
Bizuhan	1,021.26	–	23.51	76.01	0.48	–
Damot Sefatira	1,880.85	–	55.94	43.67	0.40	–
Dikulkana	1,804.48	–	52.22	47.37	0.41	–
Aklat Weybegn	2,418.72	–	34.53	62.94	2.53	–
Filatit Akabit	2,045.21	–	8.97	82.09	8.94	–
Guansit	2,261.99	–	7.11	84.16	8.73	–
Abyela Ayketuba	3,944.83	–	1.65	75.05	22.82	0.48
Gius Debtera	3,163.45	–	1.30	77.23	21.15	0.32
Agembi	1,760.86	–	10.33	78.57	11.10	–
Senebo Genetemariyam	1,918.16	–	4.56	91.39	4.05	–
Dengayber	2,797.12	–	4.59	81.98	13.42	–
Taame Abakidan	3,095.71	–	33.68	60.91	5.41	–
Tigire Debdebo	3,717.34	0.01	15.77	78.90	5.32	–
Amija Wefchana	3,518.10	–	41.42	57.37	1.21	–

and Santima Yeshoh kebeles, northern parts of Meles Misana Meda kebele, northern and northwestern parts of Shangi Dereke and Gens kebeles in the northern and northeastern parts of the study area were identified as the more vulnerable areas to flood. Abyela Ayketuba, Gius Debtera, and Senebo Genetemariyam kebeles, southern and southwestern parts of Tigire Debdebo, Telim Butila, Dengayber, Gesagis Shimbirma, Agembi, Gudiba Sekela, Taame, and Amija Wefchana kebeles, northern and northwestern parts of Guansit and Filatit Akabit kebeles in the southern and southwestern parts of the district are also more vulnerable areas to flood. These areas are mainly dominated by low elevation and relatively flat slopes, high drainage density, high rainfall amount, high flow accumulation, high TWI, and cropland land use/land cover.

By considering the percentage of area coverage from moderate to very high flood susceptibility (Table 7), Arefa Medihanialem, Chewane Bihande, Lije Nigus Chat Warka, Geshet, Chat Warka, Arefa Masikena, Damot Tsion, Fenkatit Gendawuha, Shangi Dereke, Feres Bet Michael, Gesagis Shimbirma, Filatit Akabit, Guansit, Abyela Ayketuba, Telim Butila, Gius Debtera, Senebo Genetemariyam, Agembi, and Dengayber kebeles were identified as the most susceptible kebeles to the risk of flood in the district.

On the other hand, some parts of the district such as southern and southwestern parts of Meles Misana Meda kebele, northern, northeastern, and western parts of Santima Yeshoh kebele, western and northwestern parts of Chat Warka kebele, central and northwestern parts of Gudiba Sekela kebele, northern and eastern parts of Telim Butila kebele in the western and northwestern parts of the study

area, and northern and northwestern parts of Gesagis Shimbirma kebele, southern parts of Zikuala Wegem, Dikulkana and Damot Sefatira kebeles, eastern parts of Damot TSION kebele, central part of Bizuhan kebele, northern and northeastern parts of Aklat Weybegn, Agembi, Taeme Abakidan, Tigire Debdebo, and Amija Wefchana kebeles in the southeastern parts of the district are areas with low susceptibility to flooding inundation. The areas with low flood susceptibility are dominated by high slopes and elevation, low flow accumulation, low drainage density, high NDVI, and dense vegetation cover.

Validation of the result

Model validation is essential to check whether the model output adequately represents the actual conditions on the ground/field or not. Model validation can be performed by comparing the model output with the observed flood event on the ground (Hagos et al. 2022; Mahmoud and Gan, 2018; Ogato et al. 2020; Tadesse et al. 2022). In this study, to validate the reliability of the model output, the historical flood events on the field collected from the study area Agricultural Office were compared with the locations of flood susceptible areas on the produced flood susceptibility map, and the point data collected from Google Earth were superimposed on the flood susceptibility map generated by the model.

According to Dega Damot District Agricultural Office (DDDAO 2022), Shangi Dereke, Feres Bet Michael, Gesagis Shimbirma, Geshet, Lije Nigus Chat Warka, Santima Yeshoh, Fenkatit Gendawuha, Arefa Masikena, Gudiba Sekela, and Damot TSION kebeles are the kebeles that have been frequently affected by flood hazard in the recent past years. These kebeles are also among the highly susceptible areas to flood hazards identified by the model used in this study. This means the historical flood event on the field obtained from the district agricultural office agreed well with the flood susceptibility map generated by the model used in the study or indicated the reliability of the flood susceptibility map predicted by the model. The district Agriculture Office also said that most of the kebeles located in Gumara and Muza watersheds in the northern and northeastern parts of the district have been affected by frequent flash floods in the past years, which is also directly consistent with the result of this study. During this study period, out of the kebeles identified by the model as highly vulnerable to flood, two kebeles, namely Arefa Masikana and Geshet, experienced flood events which also substantiates the reliability of the model output.

In addition, to validate the model output, point data were collected from main river plains/flood plains using Google Earth and superimposed on the flood susceptibility map (Fig. 7), which also validates the reliability of the model output. It is known that river plains are highly susceptible

to flood and the data collected from the river plains/flood plains must be placed over the highly susceptible classes on the flood susceptibility map generated by the model. Superimposing the point data collected on the output flood susceptibility map is one of the methods to validate the model output which was also employed by previous studies (Hagos et al. 2022; Ogato et al. 2020).

Conclusion

Dega Damot is one of the districts in northwestern Ethiopia susceptible to flood hazards due to heavy rainfall and its topography. This study was carried out to identify and map areas prone to flood in Dega Damot district, Northwestern Ethiopia, using the integration of geographic information system (GIS), multi-criteria decision-making (MCDM), and analytical hierarchy process (AHP). Eleven flood-controlling factors such as elevation, slope, flow accumulation, distance to rivers, rainfall, drainage density, topographic wetness index, land use land cover, Normalized Difference Vegetation Index, soil type, and curvature were computed, mapped, weighted, and overlaid together to identify and map potential flood-prone areas in the district.

The result showed that about 78.39%, 8.39%, and 0.05% of the study area experienced moderate, high, and very high susceptibility to flooding, respectively. The remaining 13.17% of the study area is characterized by low to very low susceptibility to flooding. The high and very high susceptibility to flooding was found in areas dominated by low elevation and relatively flat slope, high drainage density, rainfall amount, flow accumulation, TWI, and cropland land use/land cover.

Arefa Medihanialem, Chewane Bihande, Lije Nigus Chat Warka, Chat Warka, Geshet, Arefa Masikena, Fenkatit Gendawuha, Damot TSION, Shangi Dereke, Feres Bet Michael in the central, northern and northeastern parts of the study area; and Gesagis Shimbirma, Filatit Akabit, Guansit, Abyela Ayketuba, Gius Debtera, Senebo Genetemariyam, Agembi, Telim Butila and Dengayber kebeles in the southern and southwestern parts of the district were identified as the most susceptible kebeles to the risk of flood in the district.

In this study, the validity of the model output was evaluated by comparing the historical flood events with the model output and the historical flood events on the field agreed well with the flood susceptibility map generated by the model.

The integrated use of GIS-based multi-criteria decision-making (MCDM) and analytical hierarchy process (AHP) was found to be indispensable, less costly, and effective for the identification and mapping of areas vulnerable to flood for effective flood risk management.

Acknowledgements We would like to thank U.S Geologic Survey for enabling us to download the Sentinel 2A satellite image and the Digital Elevation Model of the study area freely from their website. We also would like to thank the Environmental System Research Institute for enabling us to download the land use and land cover map. We would like to acknowledge the National Meteorology Agency of Ethiopia and the Ethiopian Ministry of Water, Irrigation, and Energy for providing us with rainfall data and digital soil data of the study area, respectively. We also would like to acknowledge Dega Damot District Agricultural Office for its cooperation in providing the required information.

Funding The authors received no specific funding for this work.

Declaration

Conflict of interest There are no conflicts of interest.

Open Access This article is licensed under a Creative Commons Attribution 4.0 International License, which permits use, sharing, adaptation, distribution and reproduction in any medium or format, as long as you give appropriate credit to the original author(s) and the source, provide a link to the Creative Commons licence, and indicate if changes were made. The images or other third party material in this article are included in the article's Creative Commons licence, unless indicated otherwise in a credit line to the material. If material is not included in the article's Creative Commons licence and your intended use is not permitted by statutory regulation or exceeds the permitted use, you will need to obtain permission directly from the copyright holder. To view a copy of this licence, visit <http://creativecommons.org/licenses/by/4.0/>.

References

- Abdelkarim A, Al-Alola SS, Alogayell HM, Mohamed SA, Alkadi II, Ismail IY (2020) Integration of GIS-based multicriteria decision analysis and analytic hierarchy process to assess flood hazard on the Al-shamal train pathway in Al-qurayyat region, Kingdom of Saudi Arabia. *Water*. <https://doi.org/10.3390/w12061702>
- Abu Dabous S, Alkass S (2008) Decision support method for multi-criteria selection of bridge rehabilitation strategy. *Constr Manag Econ* 26(8):883–893. <https://doi.org/10.1080/01446190802071190>
- Ajibade FO, Ajibade TF, Idowu TE, Nwogwu NA, Adelodun B, Lasisi KH, Opafofa OT, Ajala OA, Fadugba OG, Adewumi JR (2021) Flood-prone area mapping using GIS-based analytical hierarchy frameworks for Ibadan city, Nigeria. *J Multi-Criteria Decis Anal*. 28(5–6):283–295. <https://doi.org/10.1002/mcda.1759>
- Ali SA, Parvin F, Pham QB, Vojtek M, Vojteková J, Costache R, Linh NTT, Nguyen HQ, Ahmad A, Ghorbani MA (2020) GIS-based comparative assessment of flood susceptibility mapping using hybrid multi-criteria decision-making approach, naïve Bayes tree, bivariate statistics and logistic regression: A case of Topľa basin, Slovakia. *Ecol Indic*. <https://doi.org/10.1016/j.ecolind.2020.106620>
- Allafta H, Opp C (2021) GIS-based multi-criteria analysis for flood prone areas mapping in the trans-boundary Shatt Al-Arab basin, Iraq-Iran. *Geomat Nat Haz Risk* 12(1):2087–2116. <https://doi.org/10.1080/19475705.2021.1955755>
- Astutik S, Pangastuti EI, Nurdin EA, Ikhsan FA, Kurnianto FA, Apriyanto B, Mujib MA (2021) Assessment of Flood Hazard Mapping Based on Analytical Hierarchy Process (AHP) and GIS: Application in Kencong District, Jember Regency, Indonesia. *Geosfera Indonesia*. <https://doi.org/10.19184/geosi.v6i3.21668>
- Aydin MC, Birincioğlu SE (2022) Flood risk analysis using gis-based analytical hierarchy process: a case study of Bitlis Province. *Appl Water Sci*. <https://doi.org/10.1007/s13201-022-01655-x>
- Binns AD (2022) Sustainable development and flood risk management. *J Flood Risk Manag*. <https://doi.org/10.1111/jfr3.12807>
- Dang ATN, Kumar L (2017) Application of remote sensing and GIS-based hydrological modelling for flood risk analysis: a case study of District 8, Ho Chi Minh city, Vietnam. *Geomat Nat Hazards Risk* 8(2):1792–1811. <https://doi.org/10.1080/19475705.2017.1388853>
- Danumah JH, Odai SN, Saley BM, Szarzynski J, Thiel M, Kwaku A, Kouame FK, Akpa LY (2016) Flood risk assessment and mapping in Abidjan district using multi-criteria analysis (AHP) model and geoinformation techniques, (cote d'ivoire). *Geoenviron Disasters*. <https://doi.org/10.1186/s40677-016-0044-y>
- Das S, Gupta A (2021) Multi-criteria decision based geospatial mapping of flood susceptibility and temporal hydro-geomorphic changes in the Subarnarekha basin, India. *Geosci Front*. <https://doi.org/10.1016/j.gsf.2021.101206>
- Dash P, Sar J (2020) Identification and validation of potential flood hazard area using GIS-based multi-criteria analysis and satellite data-derived water index. *J Flood Risk Manag*. <https://doi.org/10.1111/jfr3.12620>
- DDDAO. (2022). Dega Damot District Agricultural Office: Kebeles in Dega Damot district where flood hazard occurred in the past years. Feresbet, Ethiopia
- Demir V, Kisi O (2016) Flood Hazard mapping by using geographic information system and hydraulic model: Mert river, Samsun, Turkey. *Adv Meteorol*. <https://doi.org/10.1155/2016/4891015>
- Desalegn H, Mulu A (2021) Flood vulnerability assessment using GIS at Fetam watershed, upper Abbay basin, Ethiopia. *Heliyon* 7(1):e05865. <https://doi.org/10.1016/j.heliyon.2020.e05865>
- Elsheikh RFA, Ouerghi S, Elhag AR (2015) Flood risk map based on GIS, and multi criteria techniques (case study Terengganu Malaysia). *J Geogr Inf Syst* 07(04):348–357. <https://doi.org/10.4236/jgis.2015.74027>
- Erena SH, Worku H, De Paola F (2018) Flood hazard mapping using FLO-2D and local management strategies of Dire Dawa city, Ethiopia. *J Hydrol Reg Stud* 19:224–239. <https://doi.org/10.1016/j.ejrh.2018.09.005>
- Farhadi H, Najafzadeh M (2021) Flood risk mapping by remote sensing data and random forest technique. *Water*. <https://doi.org/10.3390/w13213115>
- Hadipour V, Vafaie F, Deilami K (2020) coastal flooding risk assessment using a GIS-based spatial multi-criteria decision analysis approach. *Water*. <https://doi.org/10.3390/w12092379>
- Hagos YG, Andualem TG, Yibeltal M, Mengie MA (2022) Flood hazard assessment and mapping using GIS integrated with multi-criteria decision analysis in upper Awash River basin, Ethiopia. *Appl Water Sci*. <https://doi.org/10.1007/s13201-022-01674-8>
- Hong H, Panahi M, Shirzadi A, Ma T, Liu J, Zhu A-X, Chen W, Kougias I, Kazakis N (2018a) Flood susceptibility assessment in Hengfeng area coupling adaptive neuro-fuzzy inference system with genetic algorithm and differential evolution. *Sci Total Environ* 621:1124–1141. <https://doi.org/10.1016/j.scitotenv.2017.10.114>
- Hong H, Tsangaratos P, Ilia I, Liu J, Zhu A-X, Chen W (2018b) Application of fuzzy weight of evidence and data mining techniques in construction of flood susceptibility map of Poyang County, China. *Sci Total Environ* 625:575–588. <https://doi.org/10.1016/j.scitotenv.2017.12.256>
- Kanani-Sadat Y, Arabsheibani R, Karimipour F, Nasser M (2019) A new approach to flood susceptibility assessment in data-scarce and ungauged regions based on GIS-based hybrid multi criteria

- decision-making method. *J Hydrol* 572:17–31. <https://doi.org/10.1016/j.jhydrol.2019.02.034>
- Karymbalis E, Andreou M, Batzakis D-V, Tsanakas K, Karalis S (2021) Integration of GIS-based multicriteria decision analysis and analytic hierarchy process for flood-hazard assessment in the Megalo Rema River Catchment (East Attica, Greece). *Sustainability*. <https://doi.org/10.3390/su131810232>
- Kazakis N, Kougias I, Patsialis T (2015) Assessment of flood hazard areas at a regional scale using an index-based approach and Analytical Hierarchy Process: application in Rhodope-Evros region, Greece. *Sci Total Environ* 538:555–563. <https://doi.org/10.1016/j.scitotenv.2015.08.055>
- Lee S, Rezaie F (2022) Data used for GIS-based flood susceptibility mapping. *Data Geol Ecol Oceanogr Space Sci Polar Sci* 41:1–15. <https://doi.org/10.22761/DJ2022.4.1.001>
- Mahmoud SH, Gan TY (2018) Multi-criteria approach to develop flood susceptibility maps in arid regions of Middle East. *J Clean Prod* 196:216–229. <https://doi.org/10.1016/j.jclepro.2018.06.047>
- Moore ID, Grayson RB, Ladson AR (1991) Digital terrain modeling: a review of hydrological, geomorphological, and biological applications. *Hydrological Process* 5:3–30
- NDRMC. (2018). Federal Democratic Republic of Ethiopia, National Disaster Risk Management Commission Flood Alert # 3. Addis Ababa, Ethiopia
- NDRMC. (2020). Federal Democratic Republic of Ethiopia, National Disaster Risk Management Commission Flood Alert # 2. Addis Ababa, Ethiopia
- Ogato GS, Bantider A, Abebe K, Geneletti D (2020) Geographic information system (GIS)-Based multicriteria analysis of flooding hazard and risk in Ambo Town and its watershed, West shoa zone, oromia regional State, Ethiopia. *J Hydrol Reg Stud*. <https://doi.org/10.1016/j.ejrh.2019.100659>
- Ozkan SP, Tarhan C (2016) Detection of flood hazard in Urban areas using GIS: Izmir Case. *Procedia Technol* 22:373–381. <https://doi.org/10.1016/j.protcy.2016.01.026>
- Rahmati O, Zeinivand H, Besharat M (2015) Flood hazard zoning in Yasooj region, Iran, using GIS and multi-criteria decision analysis. *Geomat Nat Haz Risk* 7(3):1000–1017. <https://doi.org/10.1080/19475705.2015.1045043>
- Razavi-Termeh SV, Kornejady A, Pourghasemi HR, Keesstra S (2018) Flood susceptibility mapping using novel ensembles of adaptive neuro fuzzy inference system and metaheuristic algorithms. *Sci Total Environ* 615:438–451. <https://doi.org/10.1016/j.scitotenv.2017.09.262>
- Saaty WA (1987) The analytic hierarchy process-what and how it is used. *Math Modell* 9(3–5):161–176
- Shadmehri Toosi A, Calbimonte GH, Nouri H, Alaghmand S (2019) River basin-scale flood hazard assessment using a modified multi-criteria decision analysis approach: a case study. *J Hydrol* 574:660–671. <https://doi.org/10.1016/j.jhydrol.2019.04.072>
- Son NT, Trang NTT, Bui XTD, Thi C (2021) Remote sensing and GIS for urbanization and flood risk assessment in Phnom Penh, Cambodia. *Geocarto Int*. <https://doi.org/10.1080/10106049.2021.1941307>
- Tadesse D, Suryabagavan KV, Nedaw D, Hailu BT (2022) A model-based flood hazard mapping in Itang District of the Gambella region, Ethiopia. *Geol Ecol Landsc*. <https://doi.org/10.1080/24749508.2021.2022833>
- Tamiru H, Dinka MO (2021) Artificial intelligence in geospatial analysis for flood vulnerability assessment: a case of dire Dawa Watershed, Awash Basin, Ethiopia. *Sci World J* 2021:6128609. <https://doi.org/10.1155/2021/6128609>
- Tehrany MS, Shabani F, Jebur MN, Hong H, Chen W, Xie X (2017) GIS-based spatial prediction of flood prone areas using standalone frequency ratio, logistic regression, weight of evidence and their ensemble techniques. *Geomat Nat Haz Risk* 8(2):1538–1561. <https://doi.org/10.1080/19475705.2017.1362038>
- UNDRR. (2022). Policy Brief, Ethiopia: risk-sensitive Budget review, public investment planning for disaster risk reduction and climate change adaptation. United Nations Office for Disaster Risk Reduction
- Wang Z, Lai C, Chen X, Yang B, Zhao S, Bai X (2015) Flood hazard risk assessment model based on random forest. *J Hydrol* 527:1130–1141. <https://doi.org/10.1016/j.jhydrol.2015.06.008>
- Weng CH, Xiaoxin Z, Jin H, Ling L, Yueping W, Xinheng Z, Weerasinghe R (2018) Research of AHP/DEA evaluation model for operation performance of municipal wastewater treatment plants. In: *E3S web of conferences*, vol 53. <https://doi.org/10.1051/e3sconf/20185304009>
- World Bank (2019). Disaster Risk Profile: Ethiopia. Africa Disaster Risk Financing Initiative
- Wubalem A, Tesfaw G, Dawit Z, Getahun B, Mekuria T, Jothimani M (2021) Comparison of statistical and analytical hierarchy process methods on flood susceptibility mapping: in a case study of the Lake Tana sub-basin in northwestern Ethiopia. *Open Geosci* 13(1):1668–1688. <https://doi.org/10.1515/geo-2020-0329>
- Yariyan P, Avand M, Abbaspour RA, Torabi Haghighi A, Costache R, Ghorbanzadeh O, Janizadeh S, Blaschke T (2020) Flood susceptibility mapping using an improved analytic network process with statistical models. *Geomat Nat Haz Risk* 11(1):2282–2314. <https://doi.org/10.1080/19475705.2020.1836036>
- Zhao G, Pang B, Xu Z, Yue J, Tu T (2018) Mapping flood susceptibility in mountainous areas on a national scale in China. *Sci Total Environ* 615:1133–1142. <https://doi.org/10.1016/j.scitotenv.2017.10.037>
- Zzaman RU, Nowreen S, Billah M, Islam AS (2021) Flood hazard mapping of Sangu River basin in Bangladesh using multi-criteria analysis of hydro geomorphological factors. *J Flood Risk Manag*. <https://doi.org/10.1111/jfr3.12715>

Publisher's Note Springer Nature remains neutral with regard to jurisdictional claims in published maps and institutional affiliations.